J. Fluid Mech. (2009), *vol.* 634, *pp.* 269–289.
doi:10.1017/S0022112009007228 Printed in the United Kingdom

Nonlinear aerodynamic damping of sharp-edged flexible beams oscillating at low Keulegan–Carpenter numbers

RAHUL A. BIDKAR[1], MARK KIMBER[2], ARVIND RAMAN[1]†, ANIL K. BAJAJ[1] AND SURESH V. GARIMELLA[2]

[1]Dynamic Systems and Stability Lab, School of Mechanical Engineering & Birck Nanotechnology Center, 585 Purdue Mall, Purdue University, West Lafayette, Indiana 47907, USA

[2]Thermal Microsystems Lab, School of Mechanical Engineering & Birck Nanotechnology Center, 585 Purdue Mall, Purdue University, West Lafayette, Indiana 47907, USA

(Received 2 June 2008 and in revised form 22 March 2009)

Slender sharp-edged flexible beams such as flapping wings of micro air vehicles (MAVs), piezoelectric fans and insect wings typically oscillate at moderate-to-high values of non-dimensional frequency parameter β with amplitudes as large as their widths resulting in Keulegan–Carpenter (KC) numbers of order one. Their oscillations give rise to aerodynamic damping forces which vary nonlinearly with the oscillation amplitude and frequency; in contrast, at infinitesimal KC numbers the fluid damping coefficient is independent of the oscillation amplitude. In this article, we present experimental results to demonstrate the phenomenon of nonlinear aerodynamic damping in slender sharp-edged beams oscillating in surrounding fluid with amplitudes comparable to their widths. Furthermore, we develop a general theory to predict the amplitude and frequency dependence of aerodynamic damping of these beams by coupling the structural motions to an inviscid incompressible fluid. The fluid–structure interaction model developed here accounts for separation of flow and vortex shedding at sharp edges of the beam, and studies vortex-shedding-induced aerodynamic damping in slender sharp-edged beams for different values of the KC number and the frequency parameter β. The predictions of the theoretical model agree well with the experimental results obtained after performing experiments with piezoelectric fans under vacuum and ambient conditions.

1. Introduction and background

The presence of a surrounding fluid significantly modifies the dynamics of oscillating slender sharp-edged structures commonly found in electronic cooling devices like piezoelectric fans (Kimber, Garimella & Raman 2007), in aeronautical applications like flapping wings of micro air vehicles (MAVs) (Ansari, Zbikowski & Knowles 2006) and in biological structures like insect wings. When such structures undergo large-amplitude oscillations, the surrounding fluid gives rise to fluid forces that depend nonlinearly on structural motion. In this article, we present experimental results and develop a theoretical model to understand the nonlinear aerodynamic damping of

† Email address for correspondence: raman@ecn.purdue.edu

slender sharp-edged *flexible* beams oscillating in surrounding quiescent fluid with large amplitudes comparable to their widths.

Typically, the effect of the surrounding fluid on these structures is incorporated into structural dynamics models either by using experimentally measured fluid force data or by using empirical relationships based on these fluid force data (Sarpkaya 1995). However, this approach of using experimental fluid force data is less effective when an *a priori* prediction of the structural amplitude response or an *a priori* estimate of the power consumption at resonance is required. Under these circumstances, a theoretical model which *a priori* accounts for the effect of the surrounding fluid is more useful than a theoretical model which relies on the experimental fluid force data. In this article, we develop such a theoretical model for slender sharp-edged beams, which oscillate in surrounding fluid with amplitudes comparable to their widths.

The nature of the fluid loading on an oscillating structure and the fluid flow theory used for modelling it depend on the amplitude of the structural oscillations. For structures with large characteristic lengths and relatively small oscillation amplitudes, such as flexible offshore structures, the fluid viscosity and the vortex shedding from sharp edges of the structure can be neglected (Chu 1963; Meyerhoff 1970; Fu & Price 1987). Under these circumstances, the surrounding fluid gives rise only to an added-mass effect, which modifies the natural frequencies of the structure. Conversely, flexible structures like flapping wings of MAVs and piezoelectric fans inherently operate at large amplitudes to actuate large volumes of the surrounding fluid. When structures oscillate with amplitudes comparable to their characteristic length, the effects of the fluid viscosity in inducing vortex shedding cannot be neglected. In such situations, the vortices shed from the structure's sharp edges produce a damping effect on the structural oscillations (Graham 1980). Furthermore, this damping force depends nonlinearly on the structural amplitude and frequency (Sarpkaya 1995). In this work, we are concerned with the *vortex-shedding-induced* damping in slender sharp-edged beams where the beam oscillation amplitudes are comparable to their widths. The focus is on developing experimentally validated theoretical models, which not only show the *amplitude* and *frequency* dependence of the vortex-shedding-induced aerodynamic damping but also clarify the underlying physics of vortex shedding and the associated mechanism that generates the damping force.

Two non-dimensional parameters, namely the Keulegan–Carpenter (KC) number and the frequency parameter β, have been identified as governing the phenomenon of vortex-shedding-induced damping for structures oscillating in a surrounding quiescent fluid (Keulegan & Carpenter 1958; Sarpkaya 1976). These parameters are defined as

$$KC = \frac{2\pi A}{c}, \tag{1.1}$$

and

$$\beta = \frac{c^2\omega}{2\pi\nu}, \tag{1.2}$$

where A is the amplitude of structural oscillations, c is the characteristic length of the structure, ω is the angular frequency of structural oscillations and ν is the kinematic viscosity of the fluid. The oscillatory Reynolds number (Re) for flows around such oscillating structures is the product of KC and β, and is defined as

$$Re = \frac{A\omega c}{\nu}. \tag{1.3}$$

Physically, the KC number signifies the distance that a fluid particle travels compared to the characteristic length of the structure before the fluid reverses the direction of flow, and is crucial for determining the size and the strength of the shed vortices as well as the nature of the fluid force acting on the structure (Keulegan & Carpenter 1958). The frequency parameter β (Sarpkaya 1976) signifies the importance of the unsteadiness of the fluid flow relative to the rate at which the fluid viscosity diffuses momentum in the fluid. These non-dimensional parameters were introduced to interpret experimental results on purely oscillatory flows around flat plates, cylinders and spheres in the works of Keulegan & Carpenter and Sarpkaya. These works reported the Fourier-averaged fluid forces acting on flat plates, cylinders and spheres in terms of drag and inertia coefficients, and studied the dependence of these force coefficients on the KC number and the frequency parameter β.

In the current article, we study the specific case of slender sharp-edged *flexible* beams and demonstrate the phenomenon of nonlinear aerodynamic damping in these beams. Specifically, we present experimental results for the aerodynamic damping of piezoelectric fans which are slender sharp-edged beams with low KC numbers (ranging from 0 to 4) and moderately high values of β (ranging from 300 to 1200). The corresponding oscillatory Reynolds numbers reach up to 4000. Following the experimental results, we develop a general theoretical model that combines the existing inviscid vortex-shedding fluid models (Jones 2003) and the structural beam models (Meirovitch 2000). This fluid–structure interaction model can be used for predicting the nonlinear aerodynamic damping and resonant amplitudes of slender sharp-edged beams for different values of KC and β. We point out that existing fluid–structure interaction models for studying beam oscillations in surrounding quiescent fluid are based on either a purely inviscid fluid theory (Chu 1963) (which neglects vortex-shedding from beam's sharp edges) or a purely viscous-diffusion-based fluid theory (Tuck 1969; Sader 1998), and that both models are inadequate for explaining the fluid loading on beams oscillating at large amplitudes. In this article, we show that for low KC values (ranging from 0 to 4) and moderately high β (ranging from 300 to 1200), the aerodynamic damping is mainly caused by the vortices shed from the beam's sharp edges.

At this point, we describe the difference between the direct numerical simulation (DNS) approach used in a related work (Tao & Thiagarajan 2003*a*,*b*) and the approach used here. Tao & Thiagarajan (2003*a*,*b*) study the vortex-shedding modes and the hydrodynamic damping of circular cylinders that oscillate along their axis of symmetry. They present experiments and use DNS to demonstrate the combined role of viscous diffusion and vortex-shedding-induced damping in determining the overall hydrodynamic damping of oscillating cylinders. The DNS approach in their work, although more accurate for modelling the finite Reynolds number viscous fluid flows, is time-intensive and computationally expensive. Here, we model the fluid flow around the oscillating beam structure by using a much simpler inviscid fluid theory with allowance for vortex shedding from the beam's sharp edges (Jones 2003). Furthermore, this fluid model is solved using a mesh-less boundary integral method, which is computationally less intensive when compared to the DNS approach. We show that for slender sharp-edged beams (oscillating at amplitudes comparable to their widths), the essential features of the surrounding fluid flow, the aerodynamic forces and the underlying physics can be sufficiently captured by using an inviscid fluid theory with discrete vortex shedding from the beam's sharp edges.

The remainder of this article is arranged in the following fashion. In § 2, we present experimental results of nonlinear aerodynamic damping in piezoelectric fans. In § 3,

Physical quantity (units)	Symbol	Fan 1	Fan 2	Fan 3
Length of the piezoelectric patch (mm)	L_1	20.5	22.9	28.3
Length of the fan (mm)	L	44.5	44.1	64.9
Width of the fan (mm)	c	6.40	12.7	12.6
Thickness of the shim (mm)	t_b	0.10	0.10	0.25
Thickness of the piezoelectric patch (mm)	t_p	0.42	0.40	0.55
Density of the shim (kg m^{-3})	ρ_{shim}	7850	7850	1400
Density of the piezoelectric patch (kg m^{-3})	ρ_{patch}	7800	7800	7800

TABLE 1. Geometric and material properties of the piezoelectric fans.

we develop a general theoretical model for predicting the nonlinear aerodynamic damping and the amplitude response of slender sharp-edged beams. We compare the experimental results and the theoretical predictions in § 4. In § 5, we present a physical explanation for the phenomenon of nonlinear aerodynamic damping, and finally in § 6, we summarize the findings of this work.

2. Experiments

2.1. *Objective of the experiments*

The main objective of the experiments conducted in this work is to estimate the aerodynamic damping of oscillating slender sharp-edged beams and demonstrate the phenomenon of nonlinear aerodynamic damping for these beams. This is achieved by measuring the amplitude and the phase of response of an oscillating slender sharp-edged beam while the excitation frequency is slowly swept from a value below the resonant frequency to a value above the resonant frequency. From this amplitude and phase response, the quality factor (Q-factor) is extracted by using the circle-fit method (Ewins 2000). Physically, the Q-factor represents the sharpness of the frequency response of the oscillating beam and is a measure of the amount of damping present when the beam oscillates in a particular eigenmode. Mathematically, the Q-factor equals $1/(2\zeta)$ where ζ is the damping ratio for that eigenmode (Meirovitch 2000).

The two sources of damping, namely, the structural damping and the aerodynamic damping are isolated by performing experiments in vacuum as well as in air. The Q-factor measured during the vacuum experiments is used to estimate the structural damping and the Q-factor measured during the air experiments is used to estimate the combined structural and aerodynamic damping. Using these estimates of the structural damping and the combined structural and aerodynamic damping, the aerodynamic damping can be calculated. Furthermore, this procedure for estimating the aerodynamic damping is repeated for increasing amplitudes of external excitation. With increasing external excitation, the amplitude of the oscillating beam increases, thereby allowing us to experimentally study the nonlinear dependence of the aerodynamic damping on the oscillation amplitude.

2.2. *Experimental set-up*

Piezoelectric fans (Piezo Systems Inc., Part Nos. RFN1-005, RFN1-LV-02) are used for performing all the experiments reported in this article (see figure 1 and table 1 for descriptions of the three different fans that were used). A piezoelectric fan consists of a thin flexible shim with a bonded piezoelectric patch. The fans considered in the current article are fabricated from mylar and steel shims. Under the influence of

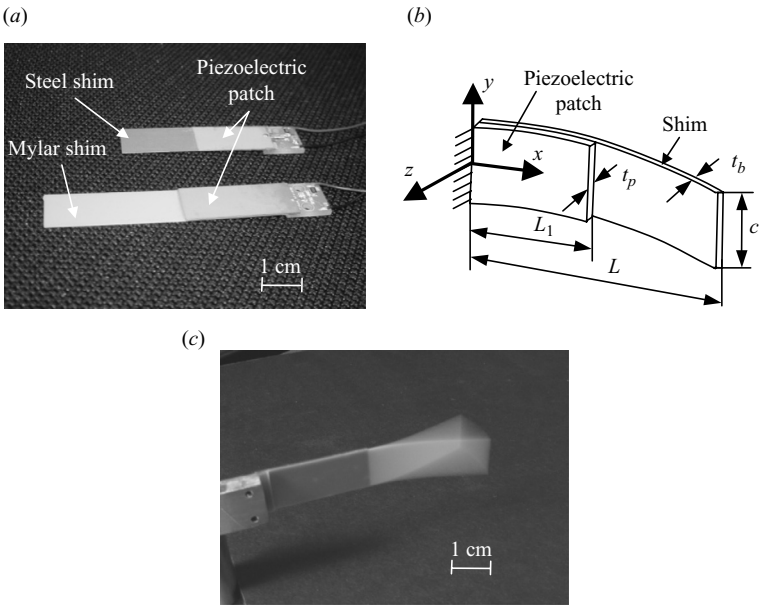

FIGURE 1. (*a*) Commercial piezoelectric fans, (*b*) a schematic diagram of a piezoelectric fan and (*c*) a picture of a piezoelectric fan oscillating with amplitudes comparable to its width.

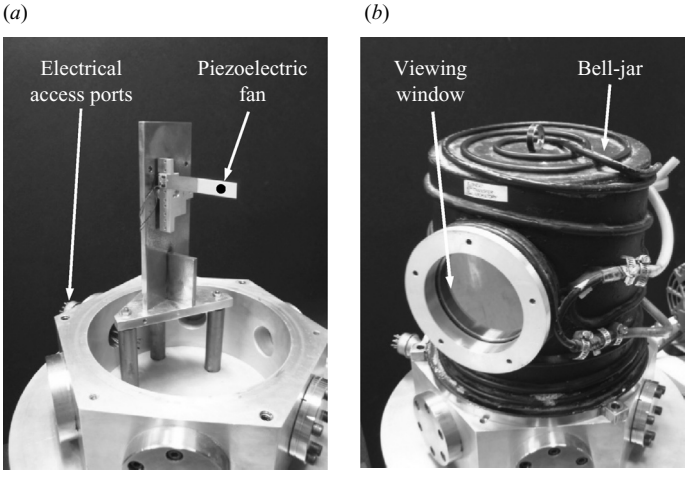

FIGURE 2. (*a*) A piezoelectric fan mounted inside the vacuum chamber and (*b*) the vacuum chamber.

an applied time-varying voltage, the piezoelectric patch applies a bending moment (about the y-axis) on the shim, and this in turn causes the transverse deflection (along the z direction) of the shim. The actuation of these piezoelectric fans is a relatively simple process and therefore these fans are ideal devices for performing experiments involving slender sharp-edged beams.

The experimental set-up is shown in figure 2. A piezoelectric fan was mounted inside a vacuum chamber, which has electrical access ports as well as optical ports. A laser displacement sensor (Model LKG-157, Keyence Corp.) was used to measure the response amplitude at a single point (the black spot in figure 2*a*) on the piezoelectric

Physical quantity (units)	Fan 1	Fan 2	Fan 3
First *in vacuo* frequency (Hz)	128	128	60
Applied voltage range (V)	5–25	5–25	5–60
Frequency range (Hz)	122–134	122–134	57–63
Free-end amplitude range (mm)	1.18–3.30	1.62–4.98	1.31–6.28

TABLE 2. Applied voltages and frequencies.

fan. The voltage signal from the laser displacement sensor was collected using a USB-based data acquisition unit (Model USB-1408FS, Measurement Computing Corp.), and the collected data were analysed using a MATLAB® program. The laser sensor could traverse along the axial direction (x-axis) of the piezoelectric fan and measure its operating deflection shape (ODS). For the vacuum experiments, the absolute pressure in the chamber was reduced to 10 Pa. The air experiments were performed in the same vacuum chamber, except under atmospheric conditions.

The experiments and the theoretical predictions presented in this article focus on the case of single mode resonant harmonic motions of piezoelectric fans because in typical electronics cooling applications such as resonant fluidic actuators (Kimber *et al.* 2007), piezoelectric fans are operated under these conditions. Specifically, we restrict our attention to studying the aerodynamic damping of piezoelectric fans oscillating in their first flexural mode (see table 2 for the first *in vacuo* resonant frequency of the three fans). The range of applied voltages, excitation frequencies and free-end oscillation amplitudes for which the experimental data were collected are shown in table 2. Experiments with the piezoelectric fans oscillating in their second flexural mode were also conducted in this work. However, two important experimental considerations give rise to a large uncertainty in the extracted values of aerodynamic damping of the second flexural mode: (*a*) unlike the first flexural mode, the amplitudes of the second mode oscillations did not change significantly between the vacuum and the air experiments, indicating that the effect of the aerodynamic damping is small compared to the structural damping, and (*b*) the response of the fan in the second mode was nonlinear in both air and vacuum, and the resonance curve exhibited a voltage-dependent bending or softening nonlinearity (Nayfeh & Mook 1979) so that the extraction of gas damping requires an accurate model of the structural nonlinearity. For these reasons, the experimental data on aerodynamic damping of the second flexural mode are not presented in this article.

2.3. *Experimental results*

In this subsection, we present experimental data on the aerodynamic damping of piezoelectric fans and also study the nonlinear dependence of this aerodynamic damping on the fan oscillation amplitude. In figure 3(*a*), we present the amplitude response curves of fan 3 (*oscillating in air*) for increasing values of the applied voltage V'. In figure 3(*b*), we replot the curves from figure 3(*a*) *with the amplitude normalized by the static deflection at zero frequency*. We see that with increased applied voltage, the *normalized* amplitude response curves of figure 3(*b*) become flatter, indicating an increase in the aerodynamic damping. The increase in damping seen in figure 3(*b*) is a predominantly aerodynamic phenomenon; this observation was verified from the vacuum experiments where the damping remains unchanged even for increased fan oscillation amplitudes. The amplitude response curves for fans 1 and 2 also show similar *amplitude-dependent* aerodynamic damping behaviour.

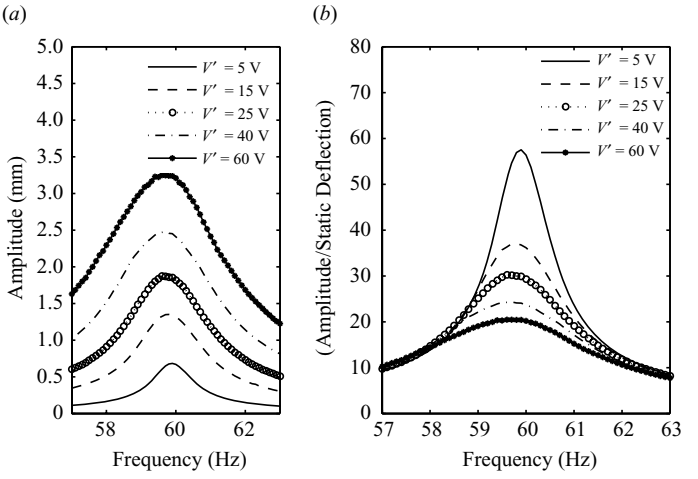

FIGURE 3. (*a*)The amplitude response of fan 3 for increasing applied voltages and (*b*) the normalized amplitude response of fan 3.

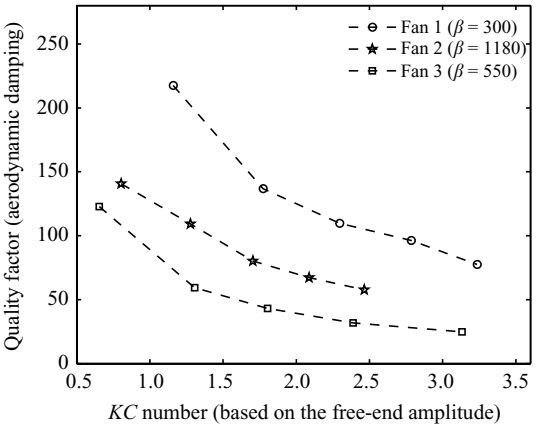

FIGURE 4. Variation of the experimentally measured Q-factor with KC number based on the free-end amplitude.

The dependence of the aerodynamic damping (represented by the corresponding Q-factor) of the three fans on the KC number is shown in figure 4. Note that the KC number used in figure 4 is based on the free-end resonant amplitude of the fan. Similarly, the values of β used in figure 4 for classifying the three fans are based on the resonant frequencies of the corresponding fans. Also, the data points shown in figure 4 represent the average values of the estimated quantities taken over a set of five experimental runs (with an average standard deviation of 0.70, 2.58 and 0.31 for fans 1, 2 and 3, respectively). This figure clearly shows that with increasing oscillation amplitude, the aerodynamic damping increases (or the Q-factor decreases) in a nonlinear fashion. In the next section, we develop a theoretical model for explaining the nonlinear aerodynamic damping results of § 2.

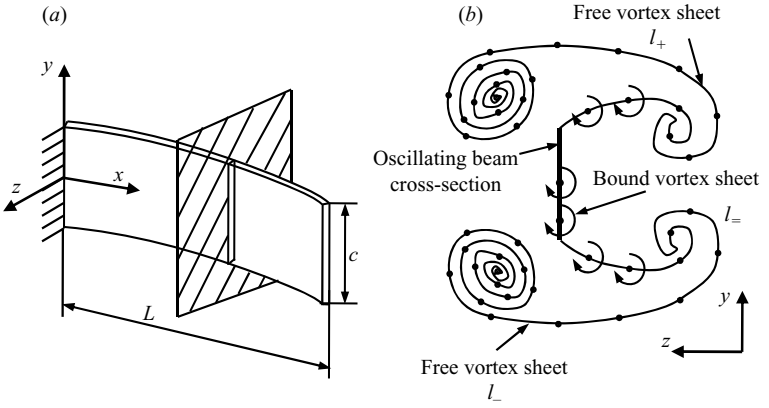

FIGURE 5. (*a*) A slender sharp-edged cantilevered beam and (*b*) the shedding of vortices from the sharp edges of the beam cross-section.

3. Development of the theoretical model

3.1. *Model*

A schematic diagram of the flexible beam along with the xyz coordinate system is shown in figure 5(*a*). The cantilever beam of width c and length L is assumed to be made of a linearly elastic and isotropic material, and its out-of-plane displacement is denoted by $w(x,t)$. Assuming that the wavelength of the motion is large and the slope of the deflection is small, the motion of the beam can be modelled using the Euler–Bernoulli beam theory:

$$EIw_{,xxxx} + \rho A_{cs} w_{,tt} = F_{fluid}(x,t) + F_{ext}(x,t), \tag{3.1}$$

where $()_{,x} = \frac{\partial()}{\partial x}$, $()_{,t} = \frac{\partial()}{\partial t}$, E represents the Young's modulus, I represents the second moment of area of the beam, ρ represents the density, A_{cs} represents the cross-sectional area, $F_{fluid}(x,t)$ represents the fluid force and $F_{ext}(x,t)$ represents the externally applied force on the beam. The structural boundary conditions for the beam are clamped at $x=0$ and free at $x=L$. We non-dimensionalize the axial direction (x direction) with the length L and the remaining two spatial directions with half-width $c/2$ of the beam. Taking the Fourier transform of (3.1), after some rearrangement we obtain:

$$w_{,xxxx}(x,\omega) - \frac{\rho A_{cs}\omega^2 L^4}{EI}\left\{ w(x,\omega) + \left(\frac{\rho_f c^2}{\rho A_{cs}}\right)\frac{F_{fluid}(x,\omega)}{\rho_f \omega^2 c^2}\right\} = \frac{L^4}{EI} F_{ext}(x,\omega), \tag{3.2}$$

where ρ_f is the fluid density and x represents the non-dimensionalized spatial variable from this point forward. In (3.2), the non-dimensional term $\frac{\rho A_{cs}\omega^2 L^4}{EI}$ characterizes the flexibility of the beam relative to the beam inertia and the fluid force. The term $\frac{\rho_f c^2}{\rho A_{cs}}$ is the non-dimensional fluid to structural mass ratio and characterizes the extent of fluid loading. In the remainder of this section, we develop a time-domain fluid flow model and then take the Fourier transform of the corresponding fluid force to calculate $F_{fluid}(x,\omega)$ corresponding to purely harmonic motion of the beam. In deriving the fluid force $F_{fluid}(x,\omega)$, it is assumed that the fluid responds instantaneously to the motion of the beam, and this assumption is justified in a later part of this article.

For developing the fluid flow model, it is assumed that the beam is surrounded by an initially quiescent, incompressible and inviscid fluid. For very large beam lengths

(when $L \gg c$), the fluid flow gradients along the x direction are far smaller than the fluid flow gradients in the remaining two directions (Taylor 1952). As a consequence, the fluid flow along the x direction is small, and it is sufficient to restrict the fluid flow problem to a two-dimensional plane parallel to the y–z plane. The governing equation for motion of the surrounding fluid is

$$\nabla^2 \phi = 0, \tag{3.3}$$

where ∇^2 is the Laplace operator and $\phi(y, z, t)$ is the velocity potential at a particular beam cross-section located at $x = x'$. The nonlinear boundary condition for the fluid flow is obtained by matching the velocity of the beam with the normal velocity of the fluid along the z direction, and is represented as

$$\phi_{,z}\,|_{surface\ of\ the\ beam} = w_{,t}\,(x', t). \tag{3.4}$$

Apart from the fluid boundary condition in (3.4), we also need to enforce the unsteady Kutta condition (Jones 2003) at the sharp edges of the beam so that the fluid flow solution becomes physically acceptable.

3.2. *Solution of the fluid flow problem*

The problem of studying the fluid flow at a particular beam cross-section (see figure 5*a*) reduces to studying the fluid flow surrounding an oscillating flat plate with two sharp-edges (see figure 5*b*). In the current work, we adapt the general solution approach developed in the work of Jones (2003) to solve the specific problem of fluid flow around an oscillating beam cross-section. In what follows, the procedure to obtain the fluid flow solution and the resulting fluid force acting on the beam cross-section is briefly summarized.

Following the work of Jones (2003), a boundary integral method is used to express the complex-conjugate velocity field $\varphi(\varsigma, t)$ (where $\varsigma = y + \mathrm{i}z$) as a combination of the flow fields caused by a beam-bound vortex sheet and two free vortex sheets emanating from the sharp edges of the beam (see figure 5*b*). Then the complex-conjugate velocity field can be written as (Jones 2003)

$$\varphi(\varsigma, t) = \frac{1}{2\pi \mathrm{i}} \left(\int_{l_-(t)} \frac{\phi_-(\lambda, t)}{\lambda - \varsigma} \mathrm{d}\lambda + \int_{l_=(t)} \frac{\phi_=(\lambda, t)}{\lambda - \varsigma} \mathrm{d}\lambda + \int_{l_+(t)} \frac{\phi_+(\lambda, t)}{\lambda - \varsigma} \mathrm{d}\lambda \right), \tag{3.5}$$

where, $l_=(t)$ represents the beam-bound vortex sheet, and $l_-(t)$ and $l_+(t)$ represent the free vortex sheets emanating from the two sharp edges of the beam cross-section. Here, $\phi_-(\lambda, t)$, $\phi_+(\lambda, t)$ and $\phi_=(\lambda, t)$ represent the complex vortex sheet strengths associated with the vortex sheets $l_-(t)$, $l_+(t)$ and $l_=(t)$, respectively. Apart from the fluid boundary conditions described in § 3.1, we require that the fluid flow perturbations caused by the beam motion decay to zero at large distances away from the beam and that the Kelvin circulation theorem is satisfied at every time instant. Furthermore, using the unsteady Kutta condition (see (3.13) in Jones 2003), we can obtain the vorticity shed into the fluid from the sharp-edges of the beam. Once the strengths of the free vortex sheets $\phi_-(\lambda, t)$ and $\phi_+(\lambda, t)$, and the strength of the bound vortex sheet $\phi_=(\lambda, t)$ are known, the fluid force acting (in the z direction) on the beam cross-section can be computed.

The solution procedure described above was implemented using a C++ program and the results of this program were benchmarked against the results presented in the work of Jones (2003). In figure 6, we present a set of representative results which were obtained after solving for the time evolution of fluid flow around a beam cross-section of non-dimensional width $c = 2$ that was undergoing the motion $w(x', t) = A\cos(\omega t)$

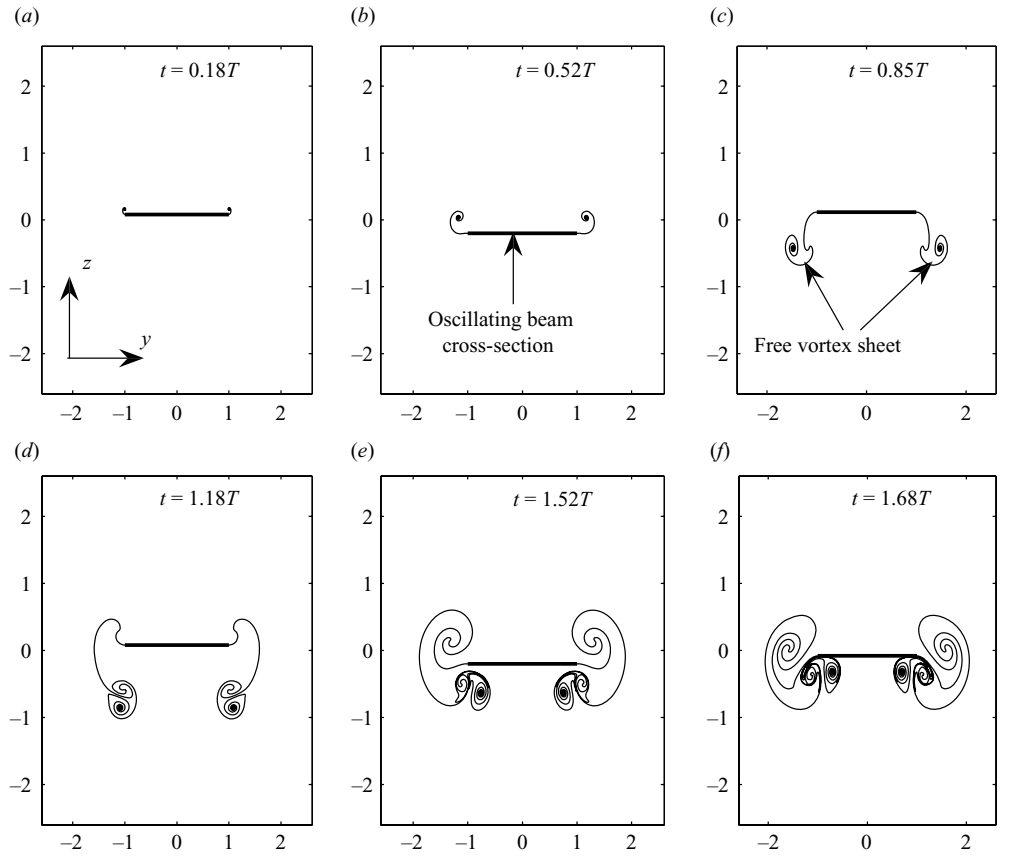

FIGURE 6. Results of a representative computation for a beam cross-section of $c = 2$ performing $w(x', t) = 0.2\cos(118\,\pi t)$. The location of the free vortex sheets are shown for time (*a*) $t = 0.18T$, (*b*) $t = 0.52T$, (*c*) $t = 0.85T$, (*d*) $t = 1.18T$, (*e*) $t = 1.52T$ and (*f*) $t = 1.68T$, where $T = 1/59$ s.

(with $A = 0.2$, $\omega = 118\pi$ rad s^{-1} and vortex-blob smoothing parameter $\delta = 0.2$ (Krasny 1986; Nitsche & Krasny 1994; Jones 2003). Figures 6(*a*)–6(*f*) show the evolution of the free vortex sheet as the beam oscillates through 1.68 cycles. Note that for beam oscillations along the z-axis, the free vortex evolution exhibits symmetry about the $y = 0$ axis even though no such constraint is imposed in the mathematical formulation. Figure 7(*a*) shows the normalized force $F(x', t)/(\rho_f A^2\omega^2 c)$ acting on the beam cross-section along with a plot of the beam acceleration $w_{,tt}(x', t)$. It is seen that the normalized force $F(x', t)/(\rho_f A^2\omega^2 c)$ *lags* the beam acceleration $w_{,tt}(x', t)$ by a small-phase angle. This phase lag between the beam acceleration and the fluid force gives rise to energy dissipation and is the main cause of the aerodynamic damping. We postpone discussion of the physical significance of this result to § 5 and first consider the approach adopted for converting the force $F(x', t)$ acting on a particular beam cross-section into the fluid force operator $F_{fluid}(x, \omega)$.

For a prescribed harmonic motion $w(x', t) = A\cos(\omega t)$ of the beam cross-section, the fluid force $F(x', t)$ is found to be periodic in time (see figure 7*b* for the normalized fluid force during the second and the third cycle superimposed on top of the fluid force during the first cycle of oscillation). The time-series fluid force data $F(x', t)$ are converted into the added mass and aerodynamic damping coefficients by representing

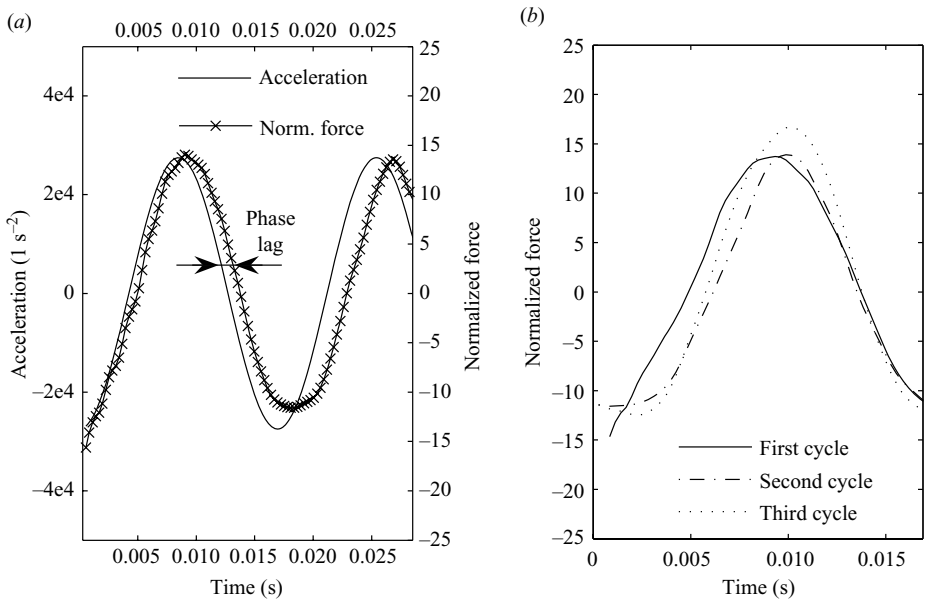

FIGURE 7. Results of a representative computation for a beam cross-section of $c = 2$ performing $w(x', t) = 0.2\cos(118\pi t)$ showing (*a*) the phase lag between the normalized fluid force and the acceleration of the beam cross-section. Note the different y-axes used for the normalized force and the acceleration, and (*b*) the computed normalized fluid force plotted with the second and the third cycles superimposed on the first cycle.

them as a Fourier series. Here we adopt the approach from the work of Keulegan & Carpenter (1958), and expand the *periodic* fluid force as a Fourier series to obtain

$$F(x', t) = -\rho_f A^2 \omega^2 c \begin{bmatrix} A_1 \cos(\omega t) + A_3 \cos(3\omega t) + A_5 \cos(5\omega t) + \cdots \\ +B_1 \sin(\omega t) + B_3 \sin(3\omega t) + B_5 \sin(5\omega t) + \cdots \end{bmatrix}, \tag{3.6}$$

where $A_n(KC)(n = 1, 3, 5, \ldots)$ and $B_n(KC)(n = 1, 3, 5, \ldots)$ are the odd Fourier series coefficients, and the even coefficients $A_2, A_4, \ldots$ and $B_2, B_4, \ldots$ are zero because of the condition $F(x', t) = -F(x', t + \pi/\omega)$. As seen in (3.6), the fluid force $F(x', t)$ depends on the amplitude A and the frequency ω through the $A^2\omega^2$ term. Additionally, the force $F(x', t)$ depends on the Fourier coefficients A_n and B_n, which in this work are known to be functions of KC alone and independent of the value of frequency ω. As a consequence, the force $F(x', t)$ depends on frequency ω only through the ω^2 term.

The Fourier series coefficients computed in the current article are based on three oscillation cycles of the beam cross-section. For low KC numbers, as is the case for the piezoelectric fans studied here, the computed fluid force reaches its steady-state periodic behaviour (see figure 7*b*) after one to two cycles of beam oscillation, and it is sufficient to use three cycles of the fluid force for computations of the Fourier coefficients. For higher KC numbers, however, a large number of beam oscillation cycles are needed to attain steady-state behaviour for the fluid force. Computational issues like the interference of the shed wake vortices and the beam cross-section (Jones 2003) do not allow the further time integration of the governing equations. Implementation of better computational schemes such as adaptive time stepping, or an improved mathematical formulation for handling the interference of the wake vortices and the beam cross-section (Jones 2003) would certainly allow further time

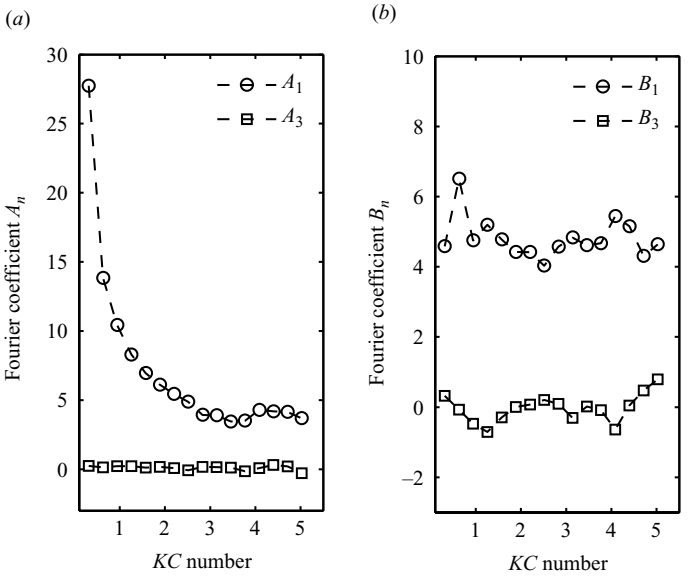

FIGURE 8. Dependence of the Fourier coefficients on the KC number (a) coefficients A_1, A_3 and (b) coefficients B_1, B_3.

integration of these equations along with better estimates for the Fourier coefficients. Such a study, however, is beyond the scope of the current article.

The dependence of the computed Fourier coefficients A_1, B_1 and A_3, B_3 on the KC number is shown in figure 8. For low values of KC, such as $KC < 10$, as is typically the case for the applications like piezoelectric fans considered here, the Fourier coefficients $A_3, A_5, \ldots$ and $B_3, B_5, \ldots$ are expected to be small (see figure 8 and Keulegan & Carpenter 1958), and the fluid force $F(x', t)$ may be well approximated by just the first harmonic of the Fourier series as

$$F(x', t) = -\rho_f A^2 \omega^2 c[A_1 \cos(\omega t) + B_1 \sin(\omega t)]. \tag{3.7}$$

Equation (3.7) is an approximate representation of the fluid force acting on a particular beam cross-section located at $x = x'$ that is performing harmonic oscillations with amplitude A. Thus, for harmonic motion of the beam cross-section and small values of KC, the fluid force $F(x', t)$ is harmonic and can be thought of as being the instantaneous response of the fluid to the beam motion. This description of the fluid force is valid for a two-dimensional beam cross-section, and needs to be coupled with the mode shape of the beam deflection so that the fluid force acting on the entire beam can be obtained. In the next subsection, we describe a procedure for converting the fluid force expression of (3.7) into a form which can be used in (3.2).

3.3. *Description of the fluid force operator* $F_{fluid}(x, \omega)$

To derive the form of the operator $F_{fluid}(x, \omega)$, we assume that the displacement of the beam *oscillating in air* can be expressed in terms of one of its *in vacuo* modes. Thus, the displacement of the beam $w(x, t)$ is

$$w(x, t) = \hat{A}_m \psi_m(x)\, \mathrm{e}^{\mathrm{i}\omega t}, \tag{3.8}$$

where $\hat{A}_m (m = 1, 2, 3, \ldots)$ is the modal participation factor, and $\psi_m(x) (m = 1, 2, 3, \ldots)$ represents any of the unit-normalized *in vacuo* modes (Meirovitch 2000) of the beam.

When $w(x,t)$ is described by (3.8), the force $F(x',t)$ from (3.7), can be written equivalently as

$$F_m(x,t) = -\rho_f \hat{A}_m^2 |\psi_m(x)| \psi_m(x) \omega^2 c (A_1 - \mathrm{i}B_1)\, \mathrm{e}^{\mathrm{i}\omega t}, \quad m = 1, 2, 3, \ldots \tag{3.9}$$

In (3.9), the $|.|$ operator on the beam mode shape is introduced to account for the dependence of the force $F_m(x,t)$ on the local displacement. After defining a *spatially varying* Keulegan–Carpenter number as $|KC(x)| = 2\pi \hat{A}_m |\psi_m(x)|/c$, we use (3.9) to obtain the following description for the Fourier transform of fluid force $F_{fluid}(x,\omega)$:

$$F_{fluid}(x,\omega) = -\left\{ -\rho_f \frac{|KC(x)|}{2\pi} \omega^2 c^2 (A_1 - \mathrm{i}B_1) w(x,\omega) \right\}. \tag{3.10}$$

The term $\rho_f \frac{|KC(x)|}{2\pi} c^2 A_1(|KC(x)|)$ is the *amplitude-dependent* added-mass coefficient, while the term $\rho_f \frac{|KC(x)|}{2\pi} \omega c^2 B_1(|KC(x)|)$ represents the *amplitude-dependent* aerodynamic damping coefficient. The fact that the Fourier coefficients A_1 and B_1 are functions of the spatially varying KC number is clearly indicated in the expressions for the added-mass and aerodynamic damping coefficients. We also note that the aerodynamic damping coefficient depends linearly on the frequency ω. Thus, very flexible beams with low resonant frequencies experience smaller aerodynamic damping compared to stiffer beams with high resonant frequencies. Substituting (3.10) into (3.2), we get:

$$w_{,xxxx}(x,\omega) - \frac{\rho A_{cs} \omega^2 L^4}{EI} \left\{ 1 + \left(\frac{\rho_f c^2}{\rho A_{cs}} \right) \frac{|KC(x)|}{2\pi} [A_1 - \mathrm{i}B_1] \right\} w(x,\omega) + \frac{\Lambda_{struct} L^4}{EI} \mathrm{i}\omega w(x,\omega) = \frac{L^4}{EI} F_{ext}(x,\omega), \tag{3.11}$$

where the coefficient Λ_{struct} has been introduced to account for the internal structural damping. In (3.11), the dependence of $A_1(|KC(x)|)$ and $B_1(|KC(x)|)$ on the spatially varying KC number is omitted for clarity. Equation (3.11) can be used for predicting the nonlinear aerodynamic damping and the amplitude response of slender sharp-edged beams under the influence of external periodic excitation $F_{ext}(x,\omega)$. The authors want to emphasize that (3.11) is valid only for harmonic motion of the beam and not for any general time-dependent motion. In the next subsection, we outline a general solution procedure for using (3.11) to obtain the amplitude response and the aerodynamic damping for a sharp-edged beam oscillating in a particular eigenmode.

3.4. *Solution procedure*

To predict the aerodynamic damping for a particular eigenmode of the beam, we use a single-mode Galerkin approximation (which uses that particular *in vacuo* eigenmode as the basis function) to transform (3.11) into an ordinary differential equation (ODE). This assumption about the single-mode approximation can be made as long as the fluid force nonlinearity does not couple the natural modes of the beam when the beam is excited with an external force. Specifically for an N-term Galerkin expansion, if ω is the excitation frequency and $\omega_1, \omega_2, \ldots, \omega_N$ are the linear natural frequencies of the beam, then mode coupling can occur if (*a*) $p\omega = q\omega_k$ (case of secondary resonances where p, q, k are integers such that both p and q cannot be 1), or (*b*) $p\omega = a_1\omega_1 + a_2\omega_2 + \cdots + a_N\omega_N$, where p and a_n are integers such that (Nayfeh & Mook 1979):

$$p + \sum_{n=1}^{n=N} |a_n| = M, \tag{3.12}$$

where M is the order of nonlinearity plus one (Nayfeh & Mook 1979). As long as these conditions are not satisfied, the beam will respond in a single mode when excited near its resonance frequency, and the use of a single-mode approximation is valid.

Expressing the beam motion in the form $w(x,\omega)=q(\omega)\psi(x)$, where $q(\omega)$ is the generalized coordinate, $\psi(x)$ is the *in vacuo* mode shape of the beam, and using Galerkin's method, the following ordinary differential equation is obtained:

$$K_s q(\omega) - \omega^2(M_s + M_f)q(\omega) + \mathrm{i}\omega(C_f + C_s)q(\omega) = F_{proj}(\omega). \tag{3.13}$$

The various terms in (3.13) are defined as follows:

$$\begin{gathered} K_s = \int_0^1 \psi(x)\psi_{,xxxx}(x)\,\mathrm{d}x, \quad M_s = \frac{L^4}{EI}\int_0^1 \rho A_{cs}\psi^2(x)\,\mathrm{d}x, \\ M_f = \frac{\rho_f c^2 L^4}{EI}\int_0^1 \frac{|KC(x)|}{2\pi} A_1(|KC(x)|)\psi^2(x)\,\mathrm{d}x, \\ C_f = \frac{\rho_f c^2 \omega L^4}{EI}\int_0^1 \frac{|KC(x)|}{2\pi} B_1(|KC(x)|)\psi^2(x)\,\mathrm{d}x, \\ F_{proj}(\omega) = \frac{L^4}{EI}\int_0^1 \psi(x)F_{ext}(x,\omega)\,\mathrm{d}x, \end{gathered} \tag{3.14}$$

while C_s has been introduced to model the internal structural damping present in the beam. For externally applied harmonic modal excitation $F_{proj}(\omega)$, the expression for the generalized coordinate becomes $q(\omega)=X_{air}\mathrm{e}^{-\mathrm{i}\theta}$, where $X_{air}(\omega)$ and $\theta(\omega)$ are the amplitude and the phase of the approximate harmonic response, respectively. Based on (3.13) the amplitude of the approximate harmonic response $X_{air}(\omega)$ of the beam oscillating in air is given by

$$X_{air}(\omega) = \frac{F_{proj}}{\sqrt{(K_s - [M_s + M_f(X_{air})]\omega^2)^2 + ([C_s + C_f(X_{air})]\omega)^2}}. \tag{3.15}$$

The terms $M_f(X_{air})$ and $C_f(X_{air})$ in (3.15) represent, respectively, the modal added-mass and the modal aerodynamic damping effects due to the surrounding air. Also, since the terms $M_f(X_{air})$ and $C_f(X_{air})$ depend on the magnitude of response $X_{air}(\omega)$, (3.15) needs to be solved iteratively in order to obtain $X_{air}(\omega)$.

Equation (3.11) is the governing equation for slender sharp-edged beams oscillating in surrounding quiescent fluid with amplitudes comparable to their widths, while equations (3.13), (3.14) and (3.15) present a procedure for predicting the amplitude response and nonlinear aerodynamic damping of such structures. These equations are quite general and can be used for a wide range of engineering applications including piezoelectric fans (Kimber *et al.* 2007), sharp-edged marine structures (Sarpkaya & Isaacson 1981), aeronautical structures like flapping-wing MAVs (Ansari *et al.* 2006), insect wings, cantilever beam wind energy harvesters and several such structures as long as these structures oscillate at low KC numbers of the order of one and perform single-mode harmonic motions.

Other extensions are possible to make this theoretical model applicable to a wider array of problems. For example, a possible extension to the current theoretical model is the inclusion of structural nonlinearities (Nayfeh & Mook 1979) and the retention of higher harmonics of the fluid force terms (see (3.6)) to study the aerodynamic dissipation of slender sharp beams oscillating at even higher KC numbers. This extension, however, is out of the scope of the current article. Before proceeding to § 4, where we compare the predictions of the current theoretical model with the

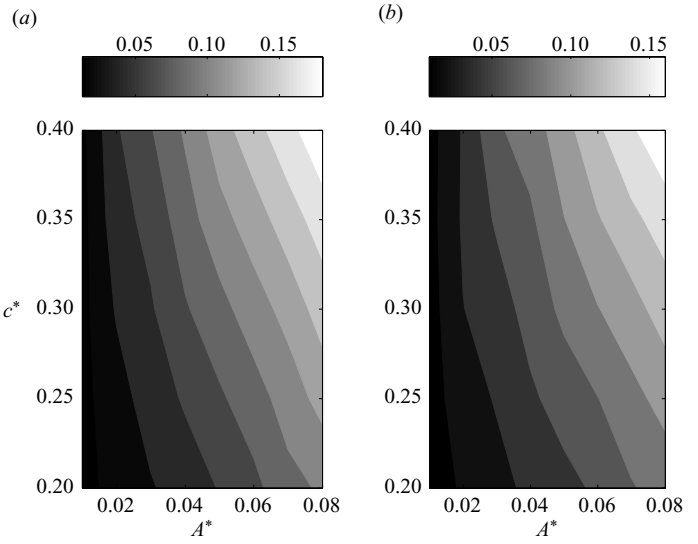

FIGURE 9. Contour plots of $C_f EI/(\rho_f \omega L^6)$ as a function of c^* and A^* for a cantilever beam oscillating in (*a*) the first mode and (*b*) the second mode.

experiments of § 2, we study the properties of the modal aerodynamic coefficient C_f, which was introduced in (3.14).

3.5. *The modal aerodynamic damping coefficient* C_f

The modal aerodynamic coefficient C_f (see (3.14)) depends on the fluid density ρ_f, the beam geometry (i.e. width c and length L), the beam oscillation mode shape $\psi(x)$ and the beam oscillation amplitude. In order to calculate C_f for a wide range of beams with different widths, lengths and oscillation amplitudes, we can normalize the expression for C_f in the following manner:

$$\frac{C_f EI}{\rho_f \omega L^6} = c^* \int_0^1 A^* B_1(|KC(\hat{x})|)|\psi(\hat{x})|\psi^2(\hat{x})\, \mathrm{d}\hat{x}. \tag{3.16}$$

In (3.16), $c^* = c/L$ is the ratio of the beam width to the beam length, $A^* = A/L$ is the ratio of the free-end beam amplitude to the beam length and $\psi(\hat{x})$ is the unit-normalized mode shape (Meirovitch 2000) of a cantilever beam.

The quantity $C_f EI/(\rho_f \omega L^6)$ can be used to predict the vortex-shedding-induced damping for a wide range of slender sharp-edged beams oscillating with amplitudes comparable to their widths. In figure 9, we plot the quantity $C_f EI/(\rho_f \omega L^6)$ as a function of c^* and A^*. Figure 9(*a*) shows a contour plot of $C_f EI/(\rho_f \omega L^6)$ for a cantilever oscillating in its first eigenmode, while figure 9(*b*) shows the contour plot of $C_f EI/(\rho_f \omega L^6)$ for the second eigenmode. From figure 9, we see that the quantity $C_f EI/(\rho_f \omega L^6)$ increases with increasing width as well as increasing free-end amplitude. The contour plots in figures 9(*a*) and 9(*b*) are quantitatively similar to one another, however, the corresponding value of aerodynamic damping C_f for the first and second mode will be different due to their different frequencies.

4. Comparison of theory and experiment

In this section, we adapt the general theoretical model for aerodynamic damping of slender sharp-edged beams developed in § 3 to the specific case of the piezoelectric

fans used in § 2. The theoretical predictions are then compared with the experimentally estimated aerodynamic damping of piezoelectric fans.

In order to determine the theoretical predictions of aerodynamic damping for piezoelectric fans (by using (3.15)), we need to know the external forcing F_{proj} (i.e. the forcing induced by the voltage-actuated piezoelectric patch) as well as the *in vacuo* mode shape and the natural frequency of the first flexural mode of the piezoelectric fan. The piezoelectric forcing can be calculated theoretically by using an analytical electro-mechanical coupling model (Bürmann, Raman & Garimella 2003), while the *in vacuo* mode shapes and natural frequencies of the piezoelectric fan can be calculated by using an accurate finite-element model of the piezoelectric fan (Wait *et al.* 2007). However, since modelling the aerodynamic damping is the primary focus of this article, we do not include an analytical model of the piezoelectric forcing or a finite-element model of the piezoelectric fan in this article. Instead, we rely on the measurements taken during the vacuum experiments for estimating the piezoelectric forcing, and the *in vacuo* mode shapes and natural frequencies. In what follows, we describe a procedure based on (3.15) for predicting the amplitude response of the piezoelectric fan.

The procedure for predicting the amplitude response $X_{air}(\omega)$ is summarized in the following discussion (see figure 10 for a detailed flow chart). We use the experimentally measured mode shape $\psi_{exp}(x)$ and the *in vacuo* resonance frequency ω_{vac} to calculate the structural modal mass M_s and the structural modal stiffness K_s of the piezoelectric fan. The structural modal damping C_s and the modal forcing F_{proj} are estimated by using the *in vacuo* amplitude response. Finally, we use the values M_s, K_s, C_s and F_{proj} along with the theoretically calculated values $M_f(X_{air})$ and $C_f(X_{air})$ to predict the response amplitude $X_{air}(\omega)$ of the piezoelectric fan. In figure 10, the two-way arrows between $X_{air}(\omega)$, and $M_f(X_{air})$ and $C_f(X_{air})$ signify the iterative nature of this calculation. Furthermore, the response amplitude $X_{air}(\omega)$ is also used to calculate the modal aerodynamic damping coefficient $C_f(X_{air})$ (and the corresponding Q-factor) of the piezoelectric fan.

Figure 11(a) shows the comparison of the theoretically predicted and the experimental amplitude response curve of fan 1 oscillating in air for an applied external voltage $V' = 5$ V. It is seen that the error in predicting the resonant frequency is 0.28 % (predicted value of 127.64 Hz and experimental value of 128.0 Hz), the error in predicting the peak amplitude is 7.94 % (predicted value of 0.9222 mm and experimental value of 1.0017 mm) and the error in predicting the Q-factor is 17.8 % (predicted value of 178.60 and experimental value of 217.45). The numbers presented here are representative calculations, and similar calculations were done for fans 1, 2 and 3 for various values of the applied voltage. Overall, the model developed in this article is capable of predicting the resonant amplitudes with an error of less than 10 %.

In figure 11(b), we show a comparison of the experimentally estimated and the theoretically predicted aerodynamic Q-factors for fans 1, 2 and 3. We see that the theoretical model slightly overpredicts (by 15 %–20 %) the aerodynamic damping. This is an expected result because the theoretical model uses a two-dimensional approximation for the fluid flow at every beam cross-section. In a three-dimensional flow, the shed vortices stretch and tilt relative to the two-dimensional computational plane (Sarpkaya 1989), and a two-dimensional vortex calculation is incapable of capturing the fluid force reduction caused by these three-dimensional effects (Sarpkaya 1989). Furthermore, the two-dimensional fluid flow assumption accounts only for vortex-shedding from the side edges of the beam, and neglects the vortex-shedding

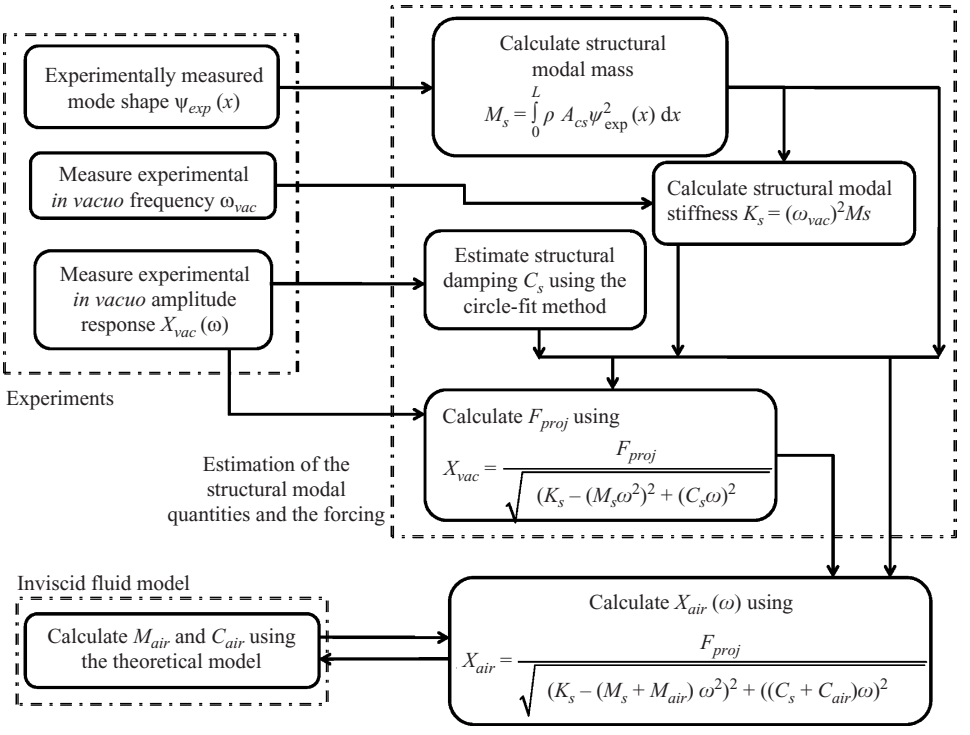

FIGURE 10. A flow-chart for combining the theoretical fluid flow model with the experimental structural model for predicting the amplitude response $X_{air}(\omega)$ of the fan.

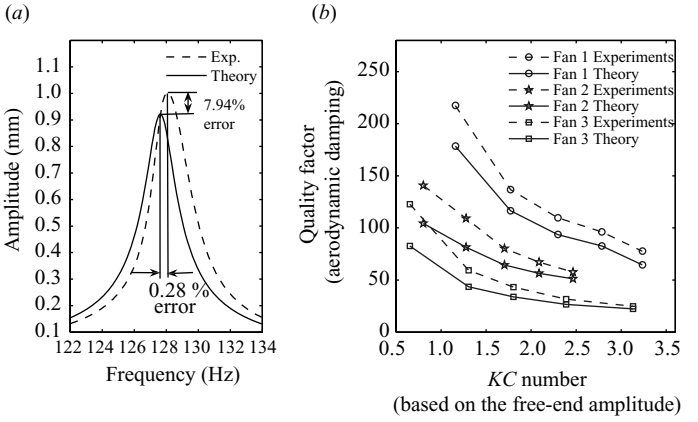

FIGURE 11. (*a*) Comparison of the theoretical and experimental amplitude response of fan 1, and (*b*) comparison of the theoretically predicted and the experimentally estimated Q-factor for fans 1, 2 and 3.

and energy dissipation at the sharp edge located at the free end ($x = L$) of the cantilever. However, since $L \gg c$, it is surmised that this effect is small compared to the side-edge vortices, and the overall effect of the two-dimensional fluid flow assumption is an over prediction of damping. Furthermore, we note that the inviscid fluid flow model presented here does not account for the viscosity-induced reduction in strength of the shed vortices, which also leads to the slight overprediction of the

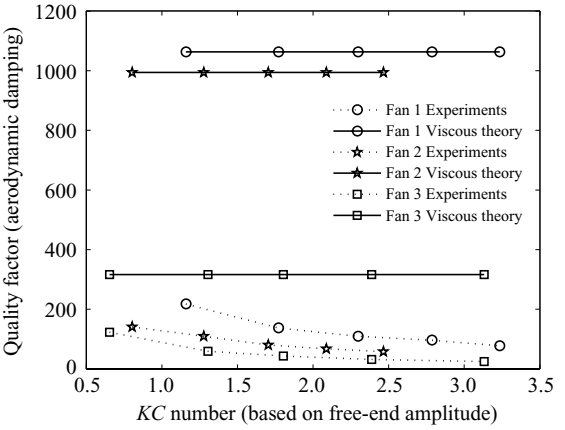

FIGURE 12. Comparison of the experimentally estimated Q-factors for fans 1, 2 and 3 with the theoretical predictions of the viscous-diffusion-based theory of Sader (1998).

aerodynamic damping. The mismatch between the theory and the air experiments is less likely to be caused due to the presence of the surrounding vacuum chamber walls, because the chamber walls are located at least 10–15 times the fan width away from the piezoelectric fan and the vortices formed around the fan are expected to diffuse before reaching the chamber walls.

It is worthwhile to compare the predictions of the current theoretical model with the predictions of the purely inviscid model of Chu (1963) and the viscous-diffusion-based model of Sader (1998). The purely inviscid model of Chu (1963) predicts that the frequencies of the piezoelectric fans 1, 2 and 3 reduce by 0.35 %, 0.70 % and 1.54 % when moved from vacuum to air due to the added mass caused by the presence of the surrounding air. Although these predictions agree well with the experimentally measured shifts in the frequencies of piezoelectric fans, the purely inviscid model (Chu 1963) is unable to predict any aerodynamic damping for these piezoelectric fans. The aerodynamic damping predictions of the viscous-diffusion-based theory (Sader 1998) can be obtained by using the fluid force expression in (9) in Sader (1998) along with the flow chart in figure 10. As shown in figure 12, the viscous-diffusion-based theory of Sader (1998) predicts Q-factors of 1063, 994 and 316 for fan 1 ($\beta = 300$), fan 2 ($\beta = 1180$) and fan 3 ($\beta = 550$), respectively, for all amplitudes of fan oscillations. These theoretical predictions show a large mismatch with the experimental results. Furthermore, the predictions of the viscous-diffusion-based theory (Sader 1998) do not depend on the amplitude of beam oscillation, thereby failing to capture the nonlinear amplitude-dependent behaviour of the aerodynamic damping. On the other hand, the current theoretical model successfully captures the nonlinear trends in aerodynamic damping with approximately 15 % error when compared to the experiments.

In summary, the theoretical model developed here is capable of predicting the nonlinear aerodynamic damping observed in slender sharp-edged beams oscillating in quiescent fluids at moderately high values of the frequency parameter β with large amplitudes comparable to their widths. The utility of the model lies in the fact that the model uses an inviscid fluid flow theory (with the advantage of less computational effort), and yet is able to capture the nonlinear trends in aerodynamic damping with approximately 15 % error when compared to the experimental values. Using a fully three-dimensional Navier–Stokes fluid model instead of the current vortex-shedding

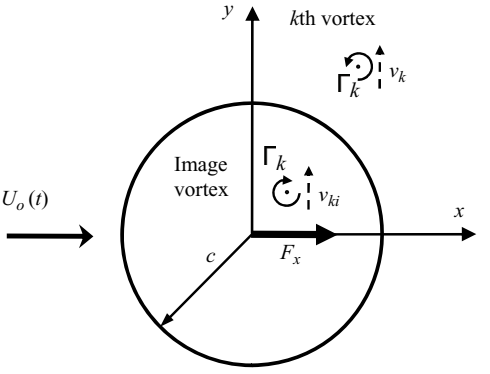

FIGURE 13. A stationary cylinder subjected to a time-dependent potential flow.

inviscid model (Jones 2003) could possibly reduce the error between theory and experiments, but only at the cost of an increased computational effort. In the next section, we present a physical explanation for the phenomenon of vortex-shedding-induced damping, which helps us better understand the trends seen in figure 11(*b*).

5. Mechanism of vortex-shedding-induced damping

It is helpful to understand the mechanism by which vortices shed by an oscillating structure in a potential flow cause the fluid force on the structure to lag its acceleration and thus dissipate structural energy. The discussion presented here complements our understanding of the phenomenon of vortex-shedding-induced damping as presented in several previous experimental (Keulegan & Carpenter 1958; Sarpkaya 1975*b*, 1976; Maull & Milliner 1978; Sarpkaya & Isaacson 1981) as well as numerical (Clements 1973; Sarpkaya 1975*a*; Stansby 1977; Jones 2003) studies.

We consider the case of a stationary cylinder of radius c (a representative case of a two-dimensional bluff body) subjected to an inviscid flow with velocity $U_o(t)$ along the x direction (see figure 13), and use this example to demonstrate how the presence of vortices around an oscillating bluff body gives rise to fluid damping. The fluid force F_x acting on the cylinder along the x direction is given by (Sarpkaya 1963)

$$F_x = 2\pi\rho_f c^2 \frac{\partial U_o}{\partial t} - \rho_f \sum_{k=1}^{m} \Gamma_k (v_k - v_{ki}), \tag{5.1}$$

where Γ_k is the real-valued strength of the kth discrete vortex (there are m such discrete vortex pairs), and v_k and v_{ki} are the y-direction transport velocities of the kth vortex and the kth image vortex, respectively.

We note from (5.1) that in the absence of vortices (i.e. $\Gamma_k = 0$) around the cylinder, the force on the cylinder is proportional only to the fluid acceleration $\partial U_o/\partial t$. However, when $\Gamma_k \neq 0$, the phase of the force component $\rho_f \Gamma_k (v_k - v_{ki})$ caused by the kth vortex pair is determined by the phase of the y-direction relative transport velocity $(v_k - v_{ki})$. In general, the relative transport velocity $(v_k - v_{ki})$ of the kth vortex pair will not be in phase with the fluid acceleration, thus causing a portion of the fluid force $\rho_f \sum_{k=1}^{m} \Gamma_k (v_k - v_{ki})$ to have a phase different from the fluid acceleration. Thus, the transport of the vortices around a cylinder with y-direction relative transport velocities $(v_k - v_{ki})$ not in phase with the fluid acceleration can shift the phase of the fluid force acting on the cylinder. For the case of a bluff body oscillating in

surrounding quiescent fluid, this phase shift between the fluid force and the structural acceleration gives rise to the vortex-shedding-induced fluid damping. Furthermore, increasing the oscillatory flow velocity $U_o(t)$ causes both the strength Γ_k of the shed vortices and the y-direction transport velocities v_k and v_{ki} to increase in magnitude, which subsequently cause the fluid force to increase in a nonlinear fashion.

6. Conclusions

Slender sharp-edged oscillating flexible beams are used as fluidic actuators in flapping wings of MAVs, insect wings and piezoelectric fans for electronics cooling, and encounter nonlinear aerodynamic forces at moderate-to-large oscillation amplitudes. This article presents detailed experiments on piezoelectric fans performed in ambient and vacuum conditions, and develops models for predicting the nonlinear aerodynamic damping for slender sharp-edged beams. In particular, both theory and experiment demonstrate that such structures encounter significant nonlinear increase in aerodynamic damping with oscillation amplitude. This behaviour is excellently captured by the model that allows for flow separation and vortex shedding from the sharp edges of the structure. The aerodynamic loading can be expressed in terms of two non-dimensional parameters KC and β making the results scalable and useful to predict the aerodynamic loading of a wide variety of sharp-edged beams oscillating in air.

REFERENCES

Ansari, S. A., Zbikowski, R. & Knowles, K. 2006 Aerodynamic modelling of insect-like flapping flight for micro air vehicles. *Prog. Aerosp. Sci.* **42**, 129–172.

Bürmann, P., Raman, A. & Garimella, S. V. 2002 Dynamics and topology optimization of piezoelectric fans. *IEEE Trans. Compon. Packag. Technol.* **25** (4), 592–600.

Chu, W. H. 1963 Vibration of fully submerged cantilever plates in water. *Tech Rep. 2*. Southwest Research Institute, TX.

Clements, R. R. 1973 Inviscid model of two-dimensional vortex shedding. *J. Fluid Mech.* **57**, 321–336.

Ewins, D. J. 2000 *Modal Testing: Theory, Practice, and Application*, 2nd ed. Baldock.

Fu, Y. & Price, W. G. 1987 Interactions between a partially or totally immersed vibrating cantilever plate and the surrounding fluid. *J. Sound Vib.* **118** (3), 495–513.

Graham, J. M. R. 1980 The forces on sharp-edged cylinders in oscillatory flow at low Keulegan–Carpenter numbers. *J. Fluid Mech.* **97** (2), 331–346.

Jones, M. A. 2003 The separated flow of an inviscid fluid around a moving flat plate. *J. Fluid Mech.* **496**, 405–441.

Keulegan, G. H. & Carpenter, L. H. 1958 Forces on cylinders and plates in an oscillating fluid. *J. Res. Natl Bur. Stand.* **60** (5), 423–440.

Kimber, M., Garimella, S. V. & Raman, A. 2007 Local heat transfer coefficients induced by piezo electrically actuated vibrating cantilevers. *J. Heat Trans.-ASME* **129**, 1168–1176.

Krasny, R. 1986 Desingulariztion of periodic vortex sheet roll-up. *J. Comput. Phys.* **65**, 292–313.

Maull, D. J. & Milliner, M. G. 1978 Sinusoidal flow past a circular cylinder. *Coast. Engng* **2**, 149–168.

Meirovitch, L. 2000 *Principles and Techniques of Vibrations*, 2nd ed. Prentice Hall.

Meyerhoff, W. K. 1970 Added mass of thin rectangular plates calculated from potential theory. *J. Ship Res.* **14**, 100–111.

Nayfeh, A. & Mook, D. 1979 *Nonlinear Oscillations*, 1st ed. John Wiley & Sons.

Nitsche, M. & Krasny, R. 1994 A numerical study of vortex ring formation at the edge of a circular tube. *J. Fluid Mech.* **276**, 139–161.

Sader, J. E. 1998 Frequency response of cantilever beams immersed in viscous fluids with applications to the atomic force microscope. *J. Appl. Phys.* **84**, 64–76.

Sarpkaya, T. 1963 Lift, drag, and added-mass coefficients for a circular cylinder immersed in a time-dependent flow. *J. Appl. Mech.-Trans. ASME* **30** (1), 13–15.

Sarpkaya, T. 1975*a* Inviscid model of two-dimensional vortex shedding for transient and asymptotically steady separated flow over an inclined flat plate. *J. Fluid Mech.* **68**, 109–128.

Sarpkaya, T. 1975*b* Forces on cylinders and spheres in a sinusoidally oscillating fluid. *J. Appl. Mech.-Trans. ASME* **42**, 32–37.

Sarpkaya, T. 1976 Vortex shedding and resistance in harmonic flow about smooth and rough circular cylinders at high Reynolds numbers. *Tech Rep.* NPS-59SL76021. Naval Postgraduate School, CA.

Sarpkaya, T. 1989 Computational methods with vortices–The 1988 Freeman scholar lecture. *J. Fluid Engng-Trans. ASME* **111**, 5–52.

Sarpkaya, T. 1995 Hydrodynamic damping, flow-induced oscillations, and biharmonic response. *J. Offshore Mech. Arct.* **117**, 232–238.

Sarpkaya, T. & Isaacson, M. 1981 *Mechanics of Wave Forces on Offshore Structures*, 1st ed. Van Nostrand Reinhold.

Stansby, P. K. 1977 Inviscid model of vortex shedding from a circular-cylinder in steady and oscillatory far flows. *P. I. Civil Engng Pt. 2* **63**, 865–880.

Tao, L. & Thiagarajan, K. 2003*a* Low KC flow regimes of oscillating sharp edges I. Vortex shedding observation. *Appl. Ocean Res.* **25**, 21–35.

Tao, L. & Thiagarajan, K. 2003*b* Low KC flow regimes of oscillating sharp edges II. Hydrodynamic forces. *Appl. Ocean Res.* **25**, 53–62.

Taylor, G. 1952 Analysis of the swimming of long and narrow animals. *Proc. R. Soc. Lond. Ser.*-A **214**, 158–183.

Tuck, E. O. 1969 Calculation of unsteady flows due to small motions of cylinders in a viscous fluid. *J. Engng Math.* **3** (1), 29–44.

Wait, S. M., Basak, S., Garimella, S. V. & Raman, A. 2007 Piezoelectric fans using higher flexural modes for electronics cooling applications. *IEEE Trans. Compon. Packag. Technol.* **30** (1), 119–128.